THE DETECTABILITY OF β PIC-LIKE CIRCUMSTELLAR DISKS AROUND NEARBY MAIN SEQUENCE STARS

PAUL KALAS AND DAVID JEWITT

Institute for Astronomy, 2680 Woodlawn Drive, Honolulu, Hawaii 96822
Electronic mail: kalas@galileo.ifa.hawaii.edu, jewitt@galileo.ifa.hawaii.edu

ABSTRACT

We model scattered light from a circumstellar disk and assess its detectability in ground-based coronagraphic observations of β Pic, Vega, and Fomalhaut. The model is fitted to the observed β Pic disk, adjusted to reflect different physical and observational parameters, and inserted into our raw data, which we subsequently reduce and evaluate for circumstellar nebulosity. We find that the prominence of the β Pic disk is primarily a result of its large scattering cross-section, rather than its edge-on inclination or close proximity to the Sun. Non-detections of disks in our coronagraphic observations of Vega and Fomalhaut imply that the total scattering cross-section of dust around these two nearby stars is not greater than a tenth of β Pic's. Our results indicate that coronagraphic surveys for circumstellar disks around main sequence stars are unlikely to produce positive results unless one order of magnitude improvement is made in the suppression of stellar light. © *1996 American Astronomical Society.*

1. INTRODUCTION

More than a decade has passed since the circumstellar dust disk around β Pic was first imaged in the optical (Smith & Terrile 1984). Even though *IRAS* data revealed that many main sequence stars possess infrared excesses due to warm orbiting particles (e.g., Aumann 1985, 1988; Backman & Gillett 1987; Backman & Paresce 1993), no circumstellar disk other than the β Pic disk has been imaged to date. For example, Smith *et al.* (1992) found no evidence for circumstellar disks around 124 main sequence stars they imaged in the optical with a coronagraph (see also Kalas & Jewitt 1993). The apparent uniqueness of β Pic stands as a major obstacle to understanding this star in the context of main sequence stellar evolution. Is β Pic unique because circumstellar disks with β Pic's outstanding inventory of dust are rare, or does β Pic simply have a favorable orientation and proximity relative to the Sun which together enhance its surface brightness and detectability relative to other *IRAS* stars?

The focus of the present paper is to explore the latter possibility by studying a model circumstellar disk. The model disk is fitted to β Pic data and therefore represents a "β Pic-like" circumstellar disk. We examine the effects of different observing geometries on the morphology and surface brightness of the disk. The surface brightness is compared to the amount of scattered light present near a star observed with and without a coronagraph. In addition, we scale the angular size of the model disk to represent β Pic as it would be seen at different distances from the Sun. We then insert these models into observational data to determine the degree to which viewing orientation and distance affect the detectability of the β Pic disk.

Next, we present coronagraphic data on Vega and Fomalhaut. Along with β Pic, these stars are described by Backman & Paresce (1993) as the "Big Three" for having the strongest and the best resolved far-infrared excesses of the main sequence stars detected by *IRAS*. They are therefore assumed to be among the most favorable main sequence stars for imaging circumstellar nebulosity. However, neither Vega nor Fomalhaut shows evidence for circumstellar material. The model disks are appropriately scaled and inserted into these data to determine if a β Pic-like disk would have been detected. By comparing the simulated data to the actual data, we place constraints on the inclinations and scattering cross-sections of disks around Vega and Fomalhaut relative to β Pic.

2. CIRCUMSTELLAR DISK MODELS

A model circumstellar disk was generated by assuming uniform particle properties and an axisymmetric number density distribution. The number density of particles at a cylindrical radius, r, and height, z, is given by

$$n(r,z) = n(r_0)\left(\frac{r}{r_0}\right)^{-\alpha} \exp\left[-\left(\frac{z/r_0}{\zeta(r)}\right)^{\gamma}\right], \qquad (1)$$

where the radial decrease in number density is approximated by a power law with index α, scaled at a fiducial distance, r_0. The number density decreases exponentially with height from the midplane if $\gamma = 1$, or as a Gaussian if $\gamma = 2$. The scale height, ζ, is a function of radius, $\zeta(r) = (\zeta_0/r_0)(r/r_0)^{\beta}$, where $\beta > 0$ is the "flare index" and ζ_0 is the scale height at r_0.

The scattering efficiency of particles is modulated by a phase function, $f(\theta)$, where θ is the phase angle (the angle subtended between the star and the observer as seen from a given particle). To obtain the intensity of scattered light we integrate through the disk in the line of sight l,

TABLE 1. Circumstellar disk candidate stars.

Star	Dates observed	Spot diam. (″)	Image quality (″)[a]	Total integration (s)	d (pc)	m_V	L/L_{sun}
HR 2020 (β Pic)	12 Oct. 1993	6.5	1.5	879	16.4	3.9	6
HR 1338	12 Oct. 1993	6.5	1.5	130	19	4.2	
HR 1998	12 Oct. 1993	6.5	1.5	225	20	3.6	
HR 7001 (α Lyr)	14 June 1994	5.0	0.7	25.5	8.1	0.03	60
HR 8728 (α PsA)	16 June 1994	4.0	0.7	22	7.0	1.2	13
	12 Oct. 1993	12.0	1.3	290			
	10 Oct. 1993	17.5	1.3	900			

[a]Measured FWHM of stellar images.

$$I = A \int_{-\infty}^{\infty} f(\theta) n(r,z) dl, \tag{2}$$

where A is a constant that is proportional to the total scattering cross-section of the grains. The transformation equations for the projection of the disk's cylindrical coordinate system into the plane of the sky are given by Artymowicz *et al.* (1989). These equations contain the disk inclination to the line of sight, i (the angle between the disk rotation axis and the plane of the sky).

Parameters of the model are adjusted to obtain an approximate fit to the β Pic disk (Sec. *4.1*). However, the model can be varied to reflect different physical conditions found at other stars. First, the brightness of the disk is adjusted to account for the luminosity difference between a given star and β Pic. Second, the linear size of the model disk is either expanded or contracted in order to represent different distances from the Sun. Third, we multiply the model by a constant factor K to simulate a uniform decrease or increase in the total scattering cross-section of the disk. This scaling accounts for possible differences in dust scattering properties, including albedo and total geometric cross-section, relative to the β Pic disk. Fourth, we incline the model disk between 0° and 90° in increments of 10°. Finally, models are convolved with a Gaussian function to simulate the seeing [full width at half maximum (FWHM) of stellar images] for a given night of data. While a Gaussian is only a rough approximation to stellar profiles in our data, the choice of convolution function has only a minor effect on the final results.

For the β Pic disk, the observed surface brightness fall off with *projected* radius, r' (AU), along the midplane can be characterized by a power law:

$$I(r') = I(r_0') \left(\frac{r'}{r_0'} \right)^{\nu}, \tag{3}$$

where $\nu \approx -3.6$ in the range 100 AU $\leqslant r' \leqslant$ 740 AU (Kalas & Jewitt 1995, hereafter referred to as Paper I). The projected radius is simply related to the angular extent, $p('')$, and the distance to the star, d(pc), by $r' = d \times p$. At a fixed p, a change in d will change r' by the same factor, changing the surface brightness by a factor of $(d_*/d_{\beta\,\text{Pic}})^{\nu}$. The scaling of each model relative to the β Pic system is therefore expressed by

$$I_*(p) = K \left(\frac{L_*}{L_{\beta\,\text{Pic}}} \right) \left(\frac{d_*}{d_{\beta\,\text{Pic}}} \right)^{\nu} I_{\beta\,\text{Pic}}(p), \tag{4}$$

where $L_*/L_{\beta\,\text{Pic}}$ represents the ratio of the R-band flux density of a given star to that of β Pic.

3. OBSERVATIONS

β Pic, Fomalhaut and Vega were observed with a broadband R filter ($\lambda_0 = 6470$ Å, $\Delta\lambda = 1250$ Å) at the University of Hawaii 2.2 m telescope on Mauna Kea (Table 1). We used a Lyot coronagraph provided by J. Gradie, B. Zuckerman, and E. Becklin, and obtained images with a Tektronix 2048 ×2048 CCD. Opaque spots of various sizes were suspended at the focal plane of the telescope to occult light from the star before it encountered any optical elements within the coronagraph. Optics in the coronagraph reimaged the pupil plane of the telescope onto an opaque Lyot stop to block light due to diffraction and scattering. Occulting spot sizes and integration times were chosen to avoid saturating the CCD, and hundreds of individual frames were typically obtained for each object. For each circumstellar disk candidate star, one or two nearby comparison stars with approximately the same visual magnitude were observed for the subtraction of scattered light and the identification of spurious features. In addition, photometric standard stars were routinely observed (Landolt 1992).

Data reduction included the standard procedures of bias subtraction, division by a flat field, and sky subtraction. Stellar images which appeared well centered on the occulting spot were then selected for coadding. Final coadded images of comparison stars were scaled and registered to the coadded images of circumstellar disk candidate stars for the final step of subtracting scattered light. The observations and data reduction for β Pic are described in greater detail in Paper I.

To characterize the effectiveness of our coronagraph in removing scattered and diffracted light, we compare images of the main sequence star 68 Oph ($m_R = 4.5$ mag) taken with and without the coronagraph on 1995 June 10 and June 11, respectively. The coronagraph reduces the median value of scattered light in fixed-width annuli by $\sim$2 mag arcsec^{-2} (Fig. 1). This empirical result falls short of theoretical predictions of up to $\sim$5 mag arcsec^{-2} suppression of diffracted light (Terrile & Ftaclas 1989). The discrepancy illustrates that scattered light due to the atmosphere, dust, and imperfections in optical components dominates the diffracted light described by theory. However, plotting the median value of scattered light as in Fig. 1 does not fully describe the improvement in image quality. The most significant advantage of using the coronagraph is the removal of multiple diffrac-
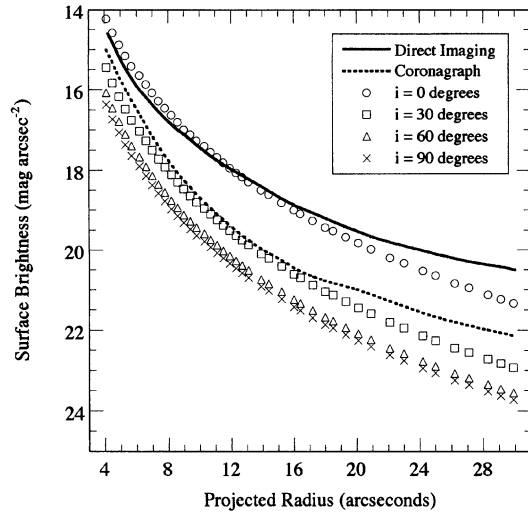
FIG. 1. Plot of the surface brightness of scattered light near 68 Oph ($m_R = +4.5$) imaged with and without a coronagraph from the same telescope, as well as the surface brightness along the midplane of a β Pic model disk at different inclinations. For the coronagraph (occulting spot diameter=5″) and direct imaging curves, we plot the median surface brightness values within successive, fixed-width annuli from 4″ to 30″ radius from the star. Because the coronagraph eliminates diffraction spikes and produces azimuthally smooth stellar profiles (cf. Fig. 2), comparison star subtractions are possible which flatten the coronagraph curve to its value at 30″. Using a larger occulting spot would also lower the coronagraph curve. The model disks show that the surface brightness of the disk diminishes by ~2 mag arcsec^{-2} when the inclination is increased from 0° to 60°, while the 90° case is only slightly fainter than the 60° case.

tion spikes (often resembling edge-on disks) that contaminate the circumstellar environment [Figs. 2(a) and 2(b)]. These diffraction spikes vary in position and in intensity and cannot be removed by a comparison star subtraction. In contrast, when the Lyot stop is properly positioned within the coronagraph, diffraction spikes are eliminated [Fig. 2(c)]. The resulting stellar images are azimuthally smooth and allow the subtraction of residual scattered light using images of comparison or artificial stars. This procedure approximately flattens the coronagraph curve in Fig. 1 to its value at 30″ radius. Therefore, the coronagraph curve shown in Fig. 1 represents an upper limit to residual contaminating light, while the direct imaging curve represents the best possible sensitivity of non-coronagraphic observations.

Observational results qualitatively indicate that data obtained with our instrumentation have a sensitivity to faint circumstellar structure which rivals that obtained by other researchers. For example, we imaged β Pic at an airmass of ~3.1 and derived basic disk properties which agreed well with those of previous studies (Paper I). In particular, we imaged the disk within 6″ radius and confirmed the inflexion of midplane surface brightness described by Golimowski et al. (1993a). We also confirmed their discovery of a star 2.1″ away from ϵ Sag (Golimowski et al. 1993b). In both cases, we imaged these southern objects at high airmass, but we matched the sensitivity of the Golimowski et al. data that were obtained at lower airmass with an adaptive optics coronagraph (Golimowski et al. 1992). Finally, we discovered an $m_R = 16.3$ mag star 5″ away from an $m_R = 5.8$ mag star HR
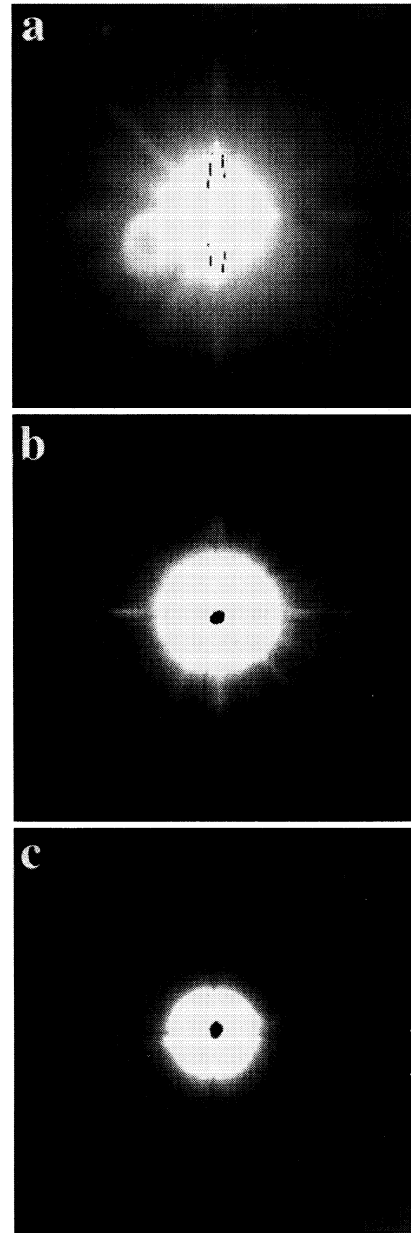

FIG. 2. Data showing the effectiveness of our coronagraph in suppressing scattered light. Panel (a) shows a $m_R = +4.5$ star imaged in R band onto the CCD with the coronagraph entirely removed. The star saturates the CCD even with an integration time of 0.4 s (we show here the result of shift-and-adding 206 frames), while diffraction spikes and internal reflections dominate the stellar environment. In panel (b), the coronagraph has been inserted at the telescope focal plane and an occulting spot blocks much of the stellar light. However, the Lyot stop has not been installed and the diffraction spikes remain. In panel (c), the Lyot stop has been inserted and adjusted to block the diffraction pattern of the telescope. Scattered light is now azimuthally smooth and can be further subtracted by fitting artificial profiles or by observing comparison stars of approximately the same magnitude.

4796 (Kalas & Jewitt 1993). This result was later confirmed by Beuzit et al. (1994) using their adaptive optics coronagraph. We therefore believe that our assessment of disk detectability is broadly representative of other ground-based coronagraphic observations.

4. MODELS APPLIED TO THREE MAIN SEQUENCE STARS

4.1 β Pic

The β Pic disk is immediately noticeable in unprocessed coronagraphic images. Using a comparison star image to subtract the stellar point-spread function (PSF) reveals the disk down to the edge of the occulting spot (radius ~4"). The northeast extension of the disk was imaged as far as 48" (790 AU) from the central star. A false-color image and surface brightness map of the disk may be found in Paper I.

Model parameter space was explored to produce good matches in isophote morphology between the model disk and our data for the northeast extension of β Pic from 6" to 40" projected radius. For this work, we chose $r_0 = 100$ AU (6") and found a good fit to the data with $i=0°$, $\alpha=-2.6$, $\gamma=1$, $\zeta_0=7$ AU, $\beta=1.2$, and a Henyey–Greenstein phase function with $|g|=0.5$ (Paper I; see also Artymowicz et al. 1989). The parameter A was determined empirically by matching the midplane surface brightnesses of the model and data at 6" radius.

Figure 1 shows the progressive drop in midplane surface brightness of the nominal β Pic disk model as the inclination is increased in 30° increments. The disk remains brighter than 20 mag arcsec^{-2} at all inclinations for $p \le 10"$ ($r' \le 164$ AU at β Pic). Comparison with the coronagraph curve demonstrates that β Pic-like disks with $0° \le i < 30°$ would be bright enough to be detected in coronagraphic data even before a comparison star subtraction is made. A comparison star subtraction would flatten the coronagraph curve, allowing the detection of light from β Pic-like disks at all inclinations. Without a coronagraph, only the $i=0°$ case would be evident.

We found that different phase functions produce significantly different disk morphologies in the range $0° < i < 40°$. Figure 3 (Plate 42) shows disk morphology and surface brightness as a function of inclination for three types of phase function. Purely isotropic scattering produces axially symmetric isophotes at all inclinations. Zodiacal particles have a strong forward scattering component. We also experimented with the Henyey–Greenstein phase function which is frequently utilized to fit the scattering properties of solids found in a variety of conditions, such as the interstellar medium (e.g., Mattila 1970), planetary atmospheres (e.g., Irvine 1975), and planetary rings (e.g., Cuzzi et al. 1984). Asymmetries between the forward scattering and backscattering directions are modulated by adjusting the value of the anisotropy parameter, g. Figure 3 shows a Henyey–Greenstein phase function where disk particles have enhanced backscattering relative to forward scattering ($g=-0.5$).

For $i \sim 0°$, disk morphology is not sensitive to the phase function, indicating that the phase function for β Pic particles is necessarily poorly constrained. However, in Paper I we found that the observed wing-tilt asymmetry is reproducible using a phase function with a moderate asymmetry between the forward and backward scattering directions, such as the Henyey–Greenstein phase function with $|g|=0.5$. We therefore adopted this phase function for our simulations.

For $i > 40°$, disk morphologies tend toward circularity and homogeneity between different phase functions. We note that

while the surface brightness of the disk may remain above detection limits (Fig. 1), the increasing similarity in morphology between the disk and the stellar PSF diminishes the probability of disk detection.

Next we explore how the model disk would appear at different inclinations in actual data. Since the β Pic data already contain a disk [Fig. 4(a)], we add the model disk to one of β Pic's disk-free comparison stars, HR 1338, which was observed at a comparable airmass [Fig. 4(b)]. A second comparison star, HR 1998, was used to subtract scattered light from the β Pic surrogate. Figures 4(a) and 4(b) (Plate 43) show good agreement between the reduced data sets for the true β Pic disk and the simulated disk (see also Paper I).

If we had chosen the Zodiacal light phase function for our simulations, then the appearance of the disk with $i=10°$ and 20° would have included a prominent forward scattering spike [Figs. 4(c) and 4(d)]. Because it is perpendicular to the disk, it could be misinterpreted as a jet, but in fact results from the scattering properties of dust. If we had used an isotropic phase function, then the disk light would have been more symmetrically arranged around the star, increasing the difficulty of distinguishing disk light from stellar light in the $40° \le i \le 60°$ cases [cf. Fig. 5 (Plate 44)]. The Henyey–Greenstein phase function chosen for our simulations produces a moderate amount of asymmetry which contributes to disk detectability at these intermediate inclinations.

Figure 5 illustrates the detectability of β Pic-like circumstellar disks as a function of inclination and stellar distance. At $d=16.4$ pc (the distance to β Pic), scattered light from the disk is evident at $0° \le i \le 30°$ because of its non-stellar, elliptical morphology. However, at $i=50°$ and 60° the disk isophotes have circularized to the point that without a priori knowledge of the existence of a disk in the data, the excess circumstellar light could also be mistaken for an imperfect subtraction of two asymmetric stellar PSFs. At $i=40°$ the circularity of disk isophotes makes a unique disk detection uncertain, but a longer effective integration time would reveal a larger area of extended structure identifiable as disk light.

Figure 5 demonstrates that the range of favorable viewing orientations becomes increasingly limited as the simulated star is placed at two, three, and four times the true distance of β Pic. At twice the distance, a firm disk detection is possible only up to $i \sim 20°$, and only up to $i \sim 10°$ when the star is placed at $d=49.2$ pc. At $d=65.6$ pc, only the edge-on case is detectable. Unfortunately, many main sequence stars purported to have circumstellar disks lie at $d > 16.4$ pc. For example, in a "Master List" of 54 main sequence stars with far-infrared excess compiled by Backman & Paresce (1993), 69% are more distant than β Pic. Our simulations indicate that the detection of circumstellar disks around the majority of "Vega-like" stars would be more observationally challenging than in the case of β Pic.

We note that according to Eq. (4), scaling the $d=16.4$ disk to $d=32.8$ pc is equivalent to scaling down the $d=16.4$ disk intensity by a factor of $K=(32.8/16.4)^{-3.6}=0.082$. Thus, the second, third, and fourth columns of Fig. 5 also approximate the β Pic disk as it might appear at 16.4 pc with 8%, 2%, and 0.7% of its original intensity (i.e., analogous to

$K = 0.08$, 0.02, and 0.007, respectively). The β Pic disk would therefore have been detected if it were uniformly 5 mag arcsec^{-2} fainter, but the detection would then be due mostly to its fortuitous edge-on inclination.

We tested two additional profile subtraction techniques to determine if any gains in detectability were possible. First, we azimuthally sampled the scattered light around the β Pic surrogate and fitted a seventh-order polynomial to generate an artificial, circularly symmetric light profile, which was then subtracted from the data. Second, we used a self-subtraction technique in which the β Pic surrogate is rotated 12 times in increments of 30° around the center of the occulting spot, and the median of these 12 images is used for a profile subtraction. The three techniques were found to be comparably effective in subtracting scattered light and there were no significant gains in disk detectability by using one technique over the other *in this data set*. We found no significant difference in the residual noise between techniques. The comparison star method has the advantage of identifying and subtracting spurious features due to instrumental scattering, but requires more observing time. However, because spurious features sometimes show disk-like morphologies, we recommend the observation of comparison stars to correctly identify the origin of circumstellar features.

4.2 Vega

Vega (HR 7001, α Lyr) is located at half the distance of β Pic and therefore a β Pic-like edge-on disk would extend to a radius of at least 90″ from the star. The thermal infrared excess from Vega can be fitted with a model dust disk or shell having an inner radius between 10″ (Aumann *et al.* 1984) and 17″ (Aumann 1991; van der Bliek *et al.* 1994). The advantage of Vega's proximity is partially offset by the fact that the star is four magnitudes brighter than β Pic, increasing the degree of atmospheric and instrumental scattered light and requiring larger occulting spots. Furthermore, spectra of Vega show a low $v \sin i$ ($\sim$22 km s^{-1}) and a nearly pole-on orientation (Gulliver *et al.* 1994), while *IRAS* scans indicate that the thermally emitting region is symmetrically arranged around the star (Gillett 1986). Pole-on disks have smaller column densities and are therefore fainter and more difficult to detect (Fig. 1). Moreover, the circular morphology of face-on disks is a major obstacle in distinguishing disk light from stellar light (Fig. 3).

Sub-arcsecond coronagraphic images of Vega were obtained as described in Table 1. The images probed to within $\sim$25 AU ($\sim$3″) of the star for circumstellar nebulosity. From 63 separate images of 1.5 s each, we selected 17 for their symmetric alignment of the stellar PSF behind the occulting spot. We used a pairwise subtraction technique where each frame of Vega was subtracted by each frame of the comparison star to find the best matches in PSFs. We then selected and median combined the 17 frames which showed the most circularly symmetric subtractions of light around Vega. The result appears to be a relatively symmetric subtraction of scattered light, though excess light remains $\sim$2″ from the edge-of the occulting spot [Fig. 6(a) (Plate 45)]. The residual halo may be the result of Vega's PSF having a different radial dependence from the PSF of the comparison star, which was

3.2 mag fainter than Vega. We conclude that the data show no convincing evidence for circumstellar nebulosity, although a circular halo of dust scattered light cannot be ruled out.

The model disk was scaled to reflect both Vega's proximity and its higher luminosity. With $K = 1$, the model disk around Vega scatters 127 times more light than the disk around β Pic at a given angular distance from the star [Table 1, Eq. (4)]. The model was then inserted into the Vega data and the results, after a comparison star subtraction, are shown in Fig. 7 (Plate 46). In the $0° \leqslant i \leqslant 40°$ models, the elongated morphology of light around the star reveals the existence of the disk. At $i > 40°$, the existence of the disk is apparent because the subtraction of a comparison star PSF cannot remove light within 10″ radius of Vega without over-subtracting the region beyond 10″ by at least 30%. Because we have never found the PSFs of two stars nearby in the sky varying to this degree on angular scales of 10″ (particularly when the measured seeing through the night is $\sim$0.8″), the modeling results would strongly indicate a nonstellar component to the residual light. Therefore, even when the morphology of the disk resembles the morphology of the stellar PSF, the disk may be detected after a comparison star subtraction if its light dominates the stellar PSF.

In models fitted to the 60 μm *IRAS* data, Backman & Paresce (1993) estimated that grains around Vega have a total geometric cross-section roughly 300 times smaller than the grains around β Pic. We scaled our model disks by factors of $K = 0.1$ and $K = 0.01$ to account for possible differences in the total scattering cross-section. With the disks scaled down by a factor of $K = 0.01$, no disk light is evident after a profile subtraction, even in the edge-on case. For disks scaled down by a factor of $K = 0.1$, disk light is evident only with $0° \leqslant i \leqslant 20°$ (Fig. 7).

We note that by setting $K = 0.1$, the higher luminosity of Vega relative to β Pic is effectively cancelled [Eq. (4)]. The $K = 0.1$ Vega simulations are therefore analogous to the β Pic disk seen at 8.1 pc. However, the range of detectable disk inclinations is found to be smaller than predicted from Fig. 5. The discrepancy indicates that our Vega data suffer from significantly greater noise than the β Pic surrogate data. The greater noise results from the necessarily shorter integration times and enhanced instrumental scattered light. Note that Vega is 4 magnitudes brighter than β Pic and HR 1338, yet we observed Vega with a smaller occulting spot (Table 1). The smaller spot was chosen to probe the circumstellar environment closer to the star than previously attempted. Unfortunately, this observing strategy reduced our potential sensitivity to β Pic-like disks.

In summary, the proximity of Vega doubles the angular extent of any β Pic-like disk, while the higher luminosity of the star increases the intensity of disk light by a factor of 10. However, our analysis shows that Vega does not possess a β Pic-like dust disk, since such a disk would be detected in our data at any inclination. Our analysis does not rule out a Vega disk with 0.1 or 0.01 the scattering cross-section of β Pic.

4.3 Fomalhaut

Gillet (1986) reported that the infrared excess of Fomalhaut (HR 8728, α Piscis Austrinus) is comparable to that of Vega in the 25 and 60 μm *IRAS* passbands, and comparable to that of β Pic at 100 μm. Scans at 60 μm showed that the emitting region is extended by 36″ at a position angle of 151°, but by less than 13″ perpendicular to this direction, indicating an orientation closer to edge-on than face-on (Gillet 1986). Aumann (1991) found a larger aspect ratio and estimated $i\sim45°$. Backman & Paresce (1993) showed that this inclination is consistent with the $v \sin i$ of Fomalhaut when compared to the mean $v \sin i$ of stars with the same spectral type. Zuckerman & Becklin (1993) mapped Fomalhaut at 800 μm and found that the emission is extended north-south with $\sim25″$ radius (P.A.=180°±30°). The improved resolution of the Infrared Space Observatory should soon elucidate the infrared morphology and orientation of the disk (Stencel & Backman 1994). Backman & Paresce (1993) estimated a total grain area for Fomalhaut which is three times that of Vega (but still two orders of magnitude less than β Pic). Compared to β Pic, Fomalhaut is approximately half as distant and twice as luminous. Therefore, a β Pic-like disk around Fomalhaut would appear 47 times brighter at a given angular radius than the β Pic disk [Table 1, Eq. (4)].

Encouraged by the reports of extended thermal emission and favorable observing parameters, we observed Fomalhaut on three different nights using occulting spots of different sizes (Table 1). No circumstellar nebulosity is evident in the data [Figs. 6(b), 6(c), and 6(d)], qualitatively confirming the result of Smith *et al.* (1992). The region probed for nebulosity is as close as ~50 AU from the star in the high signal-to-noise (S/N) data (12″ diameter spot), and ~20 AU in the low S/N data (4″ diameter spot).

The model β Pic disk was scaled to the distance and luminosity of Fomalhaut and then inserted into the data [Figs. 7 and 8 (Plate 47)]. With $K=1$, the disk is morphologically distinct up to $i=50°$, particularly because the proximity of Fomalhaut shows a large area of extended disk light at a significant distance beyond the occulting spot. The disk is evident at $i\geq60°$ because of the large amount of excess light above the stellar PSF. None of the subtractions using the real Fomalhaut data show the same degree of residual light (Fig. 6). We conclude that a disk with the size and scattering cross-section of β Pic is not present around Fomalhaut, even if $i>60°$.

With $K=0.1$, a β Pic-like disk would be morphologically evident up to $i=40°$ in the data sets shown in Fig. 8. At $i=50°$, the low S/N and poorly subtracted scattered light in the 4″ and 12″ spot data dominate the morphology of disk light. However, the high S/N in the 17.5″ spot data reveals extended disk light at a significant distance from the occulting spot, making a disk detection marginally possible. At $i\geq60°$, the disk isophotes are too circular and faint to be distinguished from the stellar PSF.

With $K=0.01$, the disk at $i=0°$ is seen in the 4″ spot data, but only marginally in the 12″ and 17.5″ spot data. At $i\geq10°$, none of the data sets show the disk. If previous es-
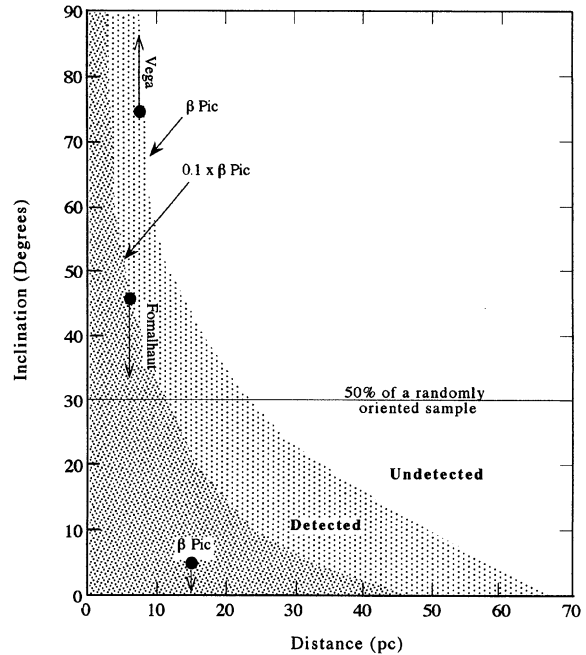

FIG. 9. Plot of the dependence of disk detectability on disk inclination and distance to the star. β Pic-like disks located in the nonshaded region would be undetectable unless they scattered more light than the β Pic disk itself. β Pic-like disks would be detectable anywhere within the shaded region, but only within the dark-shaded region if they scattered only a tenth of the light scattered by β Pic's disk. Nondetections of disks lying in the shaded region indicate that the scattering optical depth can be constrained to some fraction of β Pic's scattering optical depth. Due to their close proximity and higher stellar luminosities, β Pic-like disks around Vega and Fomalhaut would have been detected regardless of their inclination. Statistically, 50% of a randomly oriented sample of stars will fall below $i=30°$. Since most *IRAS* excess stars have $d\leq25$ pc, we expect several detections of β Pic-like disks. The non-detections from recent surveys indicate that most main sequence disks have a fraction of β Pic's scattering cross-section.

timates of Fomalhaut's inclination (e.g., $i\sim45°$) are valid, then our observational results and limited range of detectable disk inclinations in the $K=0.1$ and 0.01 simulations are consistent with the Backman & Paresce (1993) estimate for Fomalhaut's total grain area.

As with the Vega data, the range of detectable disk inclinations appears to fall short of the range predicted by the β Pic surrogate simulations (Fig. 5). For example, with $K=0.1$, the disk around Fomalhaut is still 4.7 times brighter than the β Pic surrogate disk at $K=1.0$, yet firm detections were limited to $i\leq40°$. The 4″ occulting spot data has the same noise problems described for the Vega data. The 12″ and 17.5″ spot data have a S/N comparable to that of the β Pic surrogate data, but the larger spots block a greater fraction of the bright, inner regions of the disk. According to the relation in Eq. (3), an edge-on, β Pic-like disk will be 12 times fainter at 6″ projected radius than at 3″ projected radius. When the effect of different spot sizes is taken into account, the detectability limits established for our Fomalhaut simulations are consistent with the β Pic surrogate limits. In conclusion, occulting spot sizes play a significant role in limiting disk detectability.

5. DISCUSSION

The simulated disk images demonstrate that circumstellar disks are detectable in our coronagraphic data on the basis of morphology and/or extended residual light. Figure 9 summarizes our empirically derived range of disk detectability for a β Pic-like disk, as constrained by the sensitivity of our instrumentation and data reduction procedure. A β Pic-like disk would be detectable anywhere in the shaded regions of the $i-d$ plane. When no disk is detected around a star lying within the shaded regions, the dust at a given physical distance from the star scatters at most a fraction of the total light scattered by the β Pic dust (due to a lower stellar luminosity and/or a smaller scattering cross-section). The darker-shaded region corresponds to disks which scatter a tenth of the total light scattered by β Pic's disk (i.e., 2.5 mag arcsec^{-2} fainter than β Pic at a given physical distance). Disks which scatter 100 times less light (i.e., 5.0 mag arcsec^{-2} fainter) are undetectable except in the edge-on case.

While d is relatively well-constrained for many stars closer than 50 pc, the inclinations are generally poorly known, as exemplified by even the well-studied cases Vega and Fomalhaut. However, 50% of a randomly oriented sample of circumstellar disks have inclinations between 0° and 30°. Analysis of *IRAS* coadded data has shown that ~20% of a sample of nearby A, F, and G stars ($N \sim 135$, $d < 25$ pc) possess circumstellar dust (Backman & Gillett 1987; Aumann 1988). Therefore, about 1 in 10 of this *IRAS* sample should have a disk with a favorable ($i \leq 30°$) viewing orientation. The fact that more disks have not been coronagraphically imaged (Smith *et al.* 1992; Kalas & Jewitt 1993) indicates that the scattering cross-section of dust around most stars closer than $d \sim 25$ pc is significantly less than that in the β Pic disk. This optical result is consistent with the low cross-sections of dust derived from infrared data.

In other words, the β Pic disk is observationally unique not so much because of its fortuitous edge-on inclination or its close proximity to the Sun, but because its scattering cross-section is unusually large. Figure 5 shows that the β Pic disk is bright enough tens of arcseconds away from the star for detection at $i \sim 40°$ at $d = 16.4$ pc. An edge-on orientation would be important for detectability only if β Pic were located at four times the distance, or if it had two orders of magnitude smaller scattering cross-section. The nondetections of disks around Fomalhaut and Vega (Fig. 6), combined with the modeling (Figs. 7 and 8) indicate that despite favorable values for i, d, and $L_*/L_{\beta\ \text{Pic}}$, the total scattering cross-section of dust around these systems is at least one order of magnitude less than for the β Pic disk.

Assuming similar initial conditions for star formation, explanations for the unusually large scattering cross-section of β Pic among nearby A, F, and G stars focus on either a special status (e.g., age) or a special process (e.g., the dust production mechanism). Several researchers have argued that β Pic is as young as $\sim 10^7$ yr (Jura *et al.* 1993; Lanz *et al.* 1995). This age implies that β Pic is nearing the zero-age main sequence (Nakano 1988) and that the observed disk is a remnant of the primordial accretion disk. In this scenario, the β Pic disk will resemble that of Fomalhaut or Vega millions

of years into its evolutionary future (Artymowicz 1994). Backman & Paresce (1993) describe statistical evidence consistent with this evolutionary scenario: A stars were found to have more excess infrared emission in the younger of four star clusters, indicating a decrease in main sequence circumstellar dust with age. Zuckerman & Becklin (1993) present evidence from several sub-mm surveys of young stars where dust mass appears to decrease with (time)$^{-2}$. However, for the β Pic system, the short, 10^4–10^5 yr grain-removal timescales (e.g., Beckwith *et al.* 1990, Backman & Paresce 1993), comet Halley-like shape of the silicate emission feature (Knacke *et al.* 1993), and the absence of nearby star forming regions argue against the disk as a remnant circumstellar nebula (see also Zuckerman & Becklin 1993).

The relatively short destruction time scales for micronsized dust around β Pic and other *IRAS* stars require a replenishment mechanism. This mechanism is widely believed to be the collision and/or sublimation of larger bodies such as cometesimals or asteroids (e.g., Weissman 1984; Artymowicz 1994). A similar mechanism has been proposed to explain the continued existence of our solar system's zodiacal dust particles (e.g., Sykes & Greenberg 1986) and some rings of the gas giant planets (e.g., Burns *et al.* 1984), where a balance between dust destruction and replenishment must operate. The β Pic disk may be unusually prominent or long-lived relative to disks around other *IRAS* stars if its dust replenishment mechanism is unusually robust. Observations of variable spectroscopic features (e.g., Beust *et al.* 1990), asymmetries in the spatial distribution of dust (e.g., Lagage & Pantin 1994; Paper I), and a significant vertical thickness (Zuckerman & Becklin 1993) suggest the presence of planets that may gravitationally influence the β Pic system and increase the degree of cometary activity (Beust & Morbidelli 1995; Lecavelier des Etangs *et al.* 1995). However, other main sequence systems may also contain perturbing planets (as evidenced by inner clearing zones of dust; Gillett 1986, Roques *et al.* 1994), and this mechanism does not adequately or uniquely explain β Pic's outstanding inventory of dust.

Another possibility is that both youth and the gravitational perturbations in β Pic combine to produce high dust production rates. For example, the high crater production rates among terrestrial planets 5×10^8 yr after the formation of the Sun (e.g., Soderblom *et al.* 1974) are explained by planetary perturbations on the many planetesimals still present in our young solar system. On the other hand, Wetherill (1994) has shown that an *absence* of Jovian-mass planets could result in more densely populated cometesimal systems (e.g., such as our Kuiper belt) during the early stages of solar system formation. These contradictory points demonstrate that the suggested causes for β Pic's high dust production rates are at present uncertain and speculative. We expect that data obtained with the Infrared Space Observatory will help clarify the nature of the β Pic disk in relation to other main sequence disks (Stencel & Backman 1994).

In the future, fainter main sequence disks are likely to be imaged in the optical as coronagraphic techniques advance. The potentially dramatic enhancement of image quality provided by adaptive optics (e.g., Golimowski *et al.* 1992) or space-based telescopes means that smaller occulting spots

could be used to probe regions closer to the star where disks are brightest. Improvements in image quality also provide PSFs that are better matched between stars, making the subtraction of scattered stellar light more accurate and reliable. It will then become possible to distinguish fainter face-on disks from the stellar PSF. Antiblooming CCDs, such as the one introduced by Lecavelier des Etangs *et al.* (1993), combined with improved coronagraphs would also allow smaller spots and longer integration times. Finally, suppressing at least one order of magnitude more scattered and diffracted light by improving telescope and instrument design would significantly increase the ability to image circumstellar dust. Super-smooth mirrors in telescopes, low-scattering glass in the coronagraph and camera components, and changes in the designs of the secondary spider, occulting spot, and Lyot stop have been proposed to minimize the intensity of diffracted light (e.g., Richter 1984). The *Hubble Space Telescope* was not intended to image faint objects near bright stars and suffers from many of the saturation, scattering, and diffraction problems shown in Figs. 2(a) and 2(b) (see also Malbet *et al.* 1995). However, the proposed Astrometric Imaging Telescope (Ftaclas *et al.* 1994; Pravdo *et al.* 1994) would be ideally suited for this purpose and would dramatically improve the probability of imaging circumstellar disks or planets.

6. CONCLUSIONS

Using numerical models of the β Pic disk in combination with ground-based coronagraphic data, we assessed the dependence of disk detectability on stellar distance, stellar luminosity, disk inclination, and dust scattering cross-section, all of which influence the brightness and morphology of the disk light. We found that:

(1) Increasing the inclination of the β Pic disk from 0° to 90° would decrease its surface brightness by ~ 2 mag arcsec^{-2}, but the disk would not fall below our detection limits. A more critical factor limiting the detectability of disks with high inclination (e.g., $i > 40°$) is the difficulty in separating the circular morphology of disk light from the stellar PSF (Figs. 5, 7, and 8).

(2) The large total scattering cross-section of dust is the single most important factor in revealing the β Pic disk, rather than its close proximity and near edge-on inclination. The reason β Pic has a total scattering cross-section orders of magnitude greater than that of other nearby main sequence stars remains undetermined.

(3) Axisymmetric disks which are inclined to the line of sight can have asymmetric appearances due to anisotropic dust scattering. Model disks with $10° \leqslant i < 30°$ and Zodiacal-like scattering particles produce a forward directed spike of light resembling a jet perpendicular to the disk midplane [Figs. 4(c) and 4(d)].

(4) If Vega and Fomalhaut possessed dust disks with a total scattering cross-section comparable to that of β Pic, they would have been detected in our data regardless of their inclination to the line of sight. Our model simulations indicate that the scattering cross-section of grains around Vega and Fomalhaut is no greater than a tenth of β Pic's scattering cross-section.

(5) It may be possible to detect β Pic-like disks with optical systems that improve image quality and suppress at least ten times more light than with our coronagraph. Observing programs should include the observation of comparison stars to differentiate the stellar PSF from disk light.

REFERENCES

Artymowicz, P., Burrows, C., & Paresce, F. 1989, ApJ, 337, 494
Artymowicz, P. 1994, in Proceedings of the IAP meeting "Circumstellar Dust Disks and Planet Formation," edited by R. Ferlet and A. Vidal-Madjar (Editions Frontieres, Paris), p. 47
Aumann, H. H., et al. 1984, ApJ, 278, L23
Aumann, H. H. 1985, PASP, 97, 885
Aumann, H. H. 1988, AJ, 96, 1415
Aumann, H. H. 1991, in The Infrared Spectral Region of Stars, edited by C. Jaschek and Y. Andrillat (Cambridge University Press, Cambridge), p. 363
Backman, D. E., & Gillett, F. C. 1987, in Cool Stars, Stellar Systems, and the Sun, edited by J. L. Linsky and R. E. Stencel (Springer, Berlin), p. 340
Backman, D. E., Gillett, F. C., & Witteborn, F. C. 1992, ApJ, 385, 670
Backman, D. E., & Paresce, F. 1993, in Protostars and Planets III, edited by E. H. Levy and J. I. Lunine (University of Arizona Press, Tucson), p. 1253
Beckwith, S. V. W., Sargent, A. I., Chini, R. S., & Gusten, R. 1990, AJ, 99, 924
Beust, H., Lagrange-Henri, A. M., Vidal-Madjar, A., & Ferlet, R. 1990, A&A, 236, 202
Beust, H., & Morbidelli, A. 1995, Icarus (submitted)
Beuzit, J.-L., Lagrange, A.-M., Paufique, J., & Mouillet, D. 1994, in Proceedings of the IAP meeting "Circumstellar Dust Disks and Planet Formation," edited by R. Ferlet and A. Vidal-Madjar (Editions Frontieres, Paris), p. 165
Burns, J. A., Showalter, M. R., & Morfill, G. E. 1984, in Planetary Rings, edited by R. Greenberg and A. Brahic (University of Arizona Press, Tucson), p. 200
Cuzzi, J. N., et al. 1984, in Planetary Rings, edited by R. Greenberg and A. Brahic (University of Arizona Press, Tucson), p. 73
Ftaclas, C., Nonnenmacher, A. L., Terrile, R. J., Pravdo, S. H., Gatewood, G. D., & Levy, E. H. 1994, Ap&SS, 212, 441
Gillett, F. C. 1986, in Light on Dark Matter, edited by F. P. Israel (Reidel, Dordrecht), p. 61
Golimowski, D. A., Clampin, M., Durrance, S. T., & Barkhouser, R. H. 1992, Appl. Opt. 31, 4405
Golimowski, D. A., Durrance, S. T., & Clampin, M. 1993a, ApJ, 411, L41
Golimowski, D. A., Durrance, S. T., & Clampin, M. 1993b, ApJ, 105, 1108
Gulliver, A. F., Hill, G., & Adelman, S. J. 1994, ApJ, 429, L81
Jura, M., Zuckerman, B., Becklin, E. E., & Smith, R. C. 1993, ApJ, 418, L37
Irvine, W. M. 1975, Icarus, 25, 175
Kalas, P., & Jewitt, D. 1993, BAAS, 25, 1353
Kalas, P., & Jewitt, D. 1995, AJ, 110, 794 (Paper I)
Knacke, R. F., Fajardo-Acosta, S. B., Telesco, C. M., Hackwell, J. A., Lynch, D. K., & Russel, R. W. 1993, ApJ, 418, 440
Lagage, P. O., & Pantin, E. 1994, Nature, 369, 628
Landolt, A. U. 1992, AJ, 104, 340
Lanz, R., Heap, S. R., & Hubeny, I. 1995, ApJ, 447, L41
Lecavelier des Etangs, et al. 1993, A&A, 274, 877

Lecavelier des Etangs, A, Vidal-Madjar, A., & Ferlet, R. 1995, A&A (in press)

Malbet F., Yu, J. W., & Shao, M. 1995, PASP, 107, 386

Mattila, K. 1970, A&A, 9, 53

Nakano, T. 1988, MNRAS, 230, 551

Pravdo, S. H., Terrile, R., Ftaclas, C., Gatewood, G. D., & Levy, E. H. 1994, Ap&SS, 212, 433

Richter, J. L. 1984, Appl. Opt. 23, 1907

Roques, F., Scholl, H., Sicardy, B., & Smith, B. 1994, Icarus, 108, 37

Smith, B. A., & Terrile, R. J. 1984, Science, 226, 1421

Smith, B. A., Fountain, J. W., & Terrile, R. J. 1992, A&A, 261, 499

Soderblom, L. A., Condit, C. D., West, R. A., Hermans, B. M., & Kreidler, T. J. 1974, Icarus, 22, 239

Stencel, R. E., & Backman, D. E. 1994, Ap&SS, 212, 417

Sykes, M. V., & Greenberg, R. 1986, Icarus, 65, 51

Terrile, R. J., & Ftaclas, C. 1989, SPIE, 1113, 50

van der Bliek, N. S., Prusti, T., & Waters, L. B. F. M. 1994, A&A, 285, 229

Weissman, P. R. 1984, Science, 224, 987

Wetherill, G. W. 1994, Ap&SS, 212, 23

Zuckerman, B., & Becklin, E. E. 1993, ApJ, 414, 793

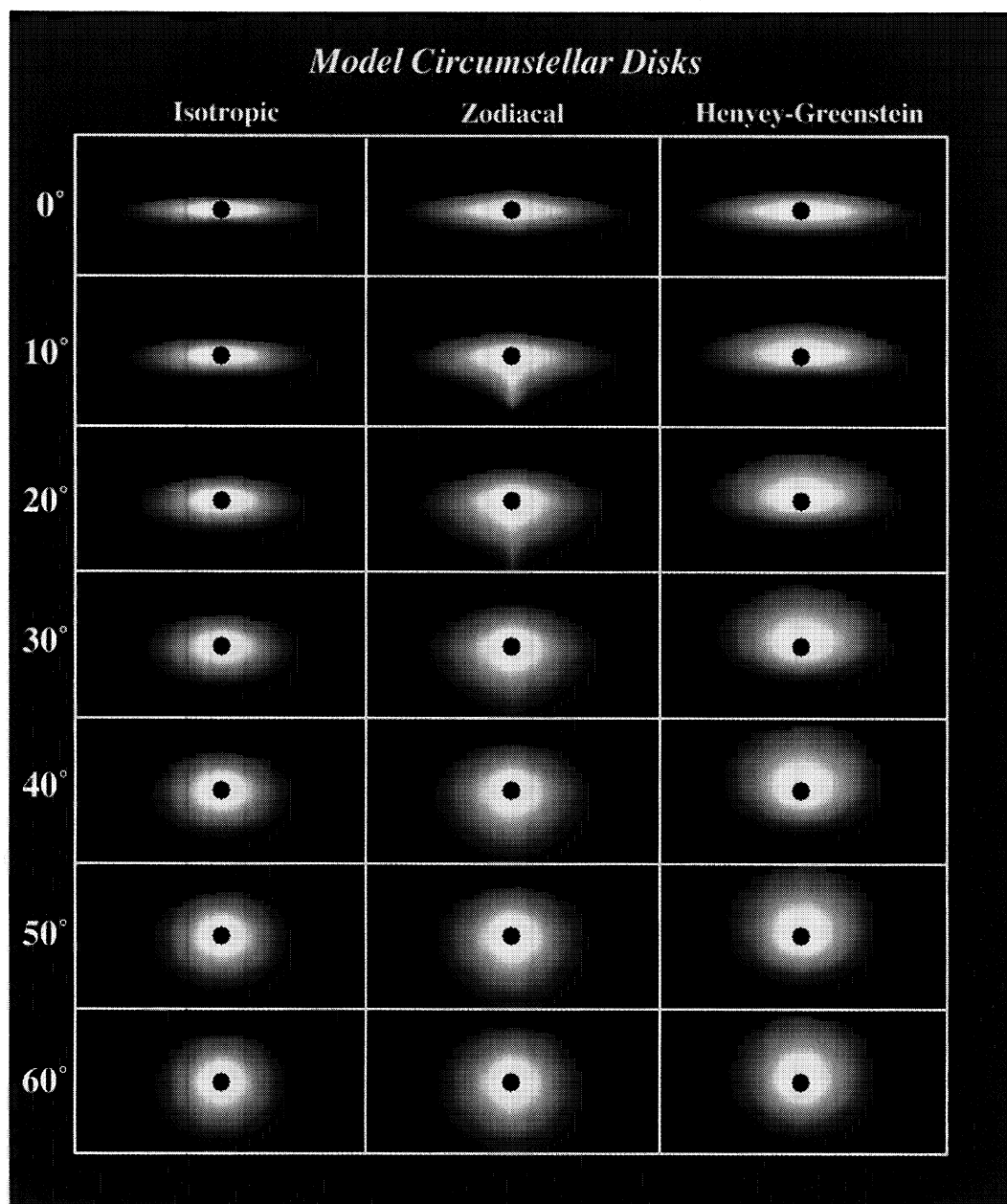PLATE 42

FIG. 3. Inclination versus phase function for scattered light models of an axisymmetric disk fit to our β Pic data. Each panel measures $80''\times40''$ and the outer boundary of the models represents the 24 mag arcsec^{-2} isophote. Edge-on models ($i=0°$) which simulate the observed β Pic surface brightness have significantly different, phase function dependent morphologies at nonzero inclinations. Models in the left-hand column use an isotropic phase function and show axisymmetric morphologies with increasing inclination. Models in the middle column use the empirically determined phase function of Zodiacal light, which has a strong forward scattering component. Models in the right-hand column use a Henyey–Greenstein phase function with enhanced backscatter over forward scatter ($g=-0.5$).
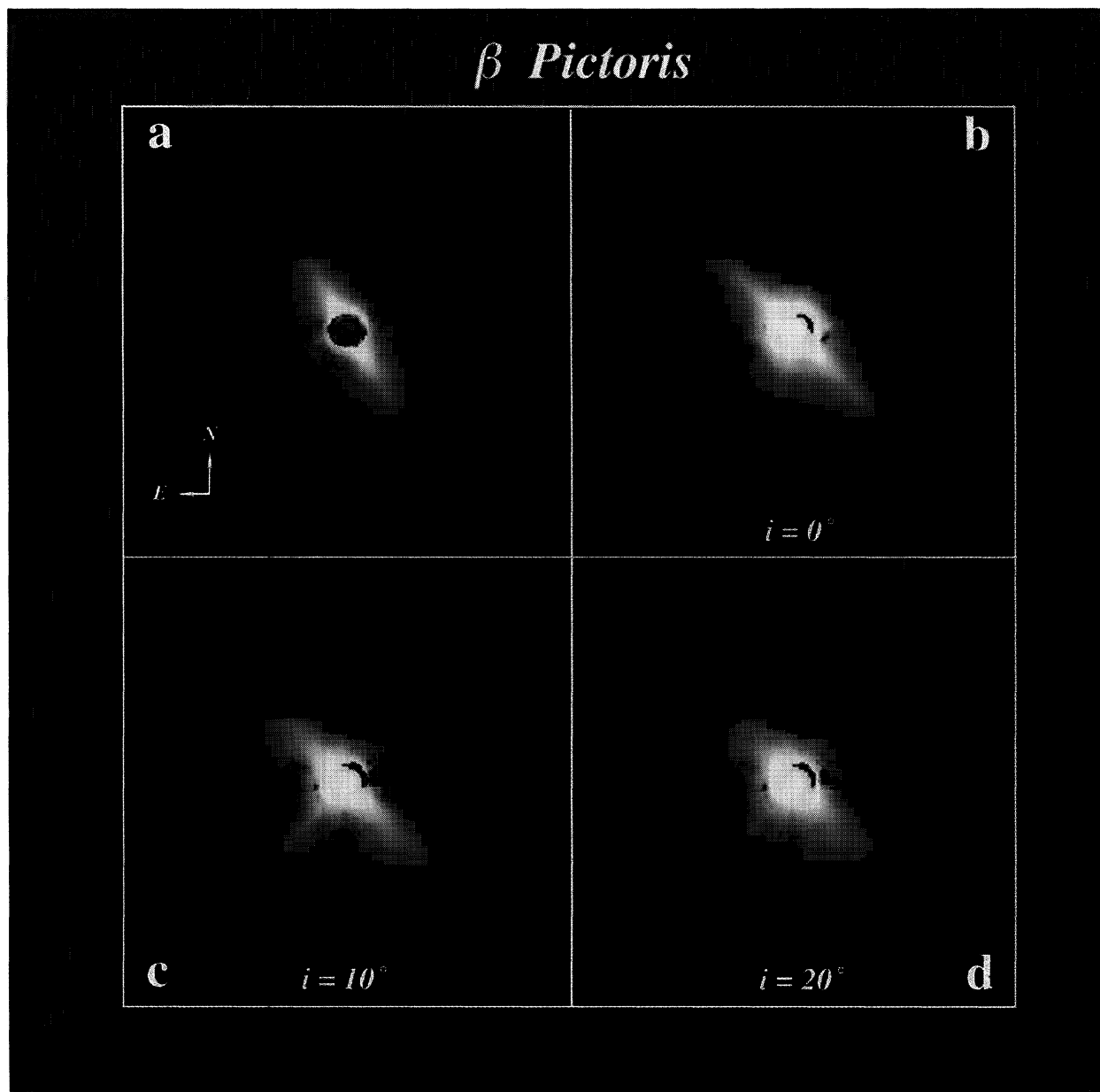
P. Kalas and D. Jewitt (see page 1350)

1422

PLATE 43

FIG. 4. A comparison of our highest signal-to-noise, R-band β Pic image in panel (a), next to the β Pic simulation in panel (b) (HR 1338 with a model disk inserted at P.A.=45°). The images were scaled from 25 to 12 mag arcsec^{-2} and each panel has a field of view of 80″×80″. The model data simulate the true β Pic data well, but the model disk appears truncated at a smaller radius because the HR 1338 data have a shorter effective integration time and a factor of 2.5 more noise than the β Pic data. Panels (c) and (d) simulate the appearance of the β Pic disk if it were inclined by 10° and 20°, respectively, and if its dust had the same phase function as our solar system's Zodiacal light. The strong forward scattering component of the Zodiacal phase function produces a prominent spike across the disk in the line of sight (disappearing at $i>30°$) which could be mistaken for a jet.

P. Kalas and D. Jewitt (see page 1350)

1423

PLATE 44

β Pictoris

d = 16.4 pc   d = 32.8 pc   d = 49.2 pc   d = 65.6 pc

i = 0°

i = 10°

i = 20°

i = 30°
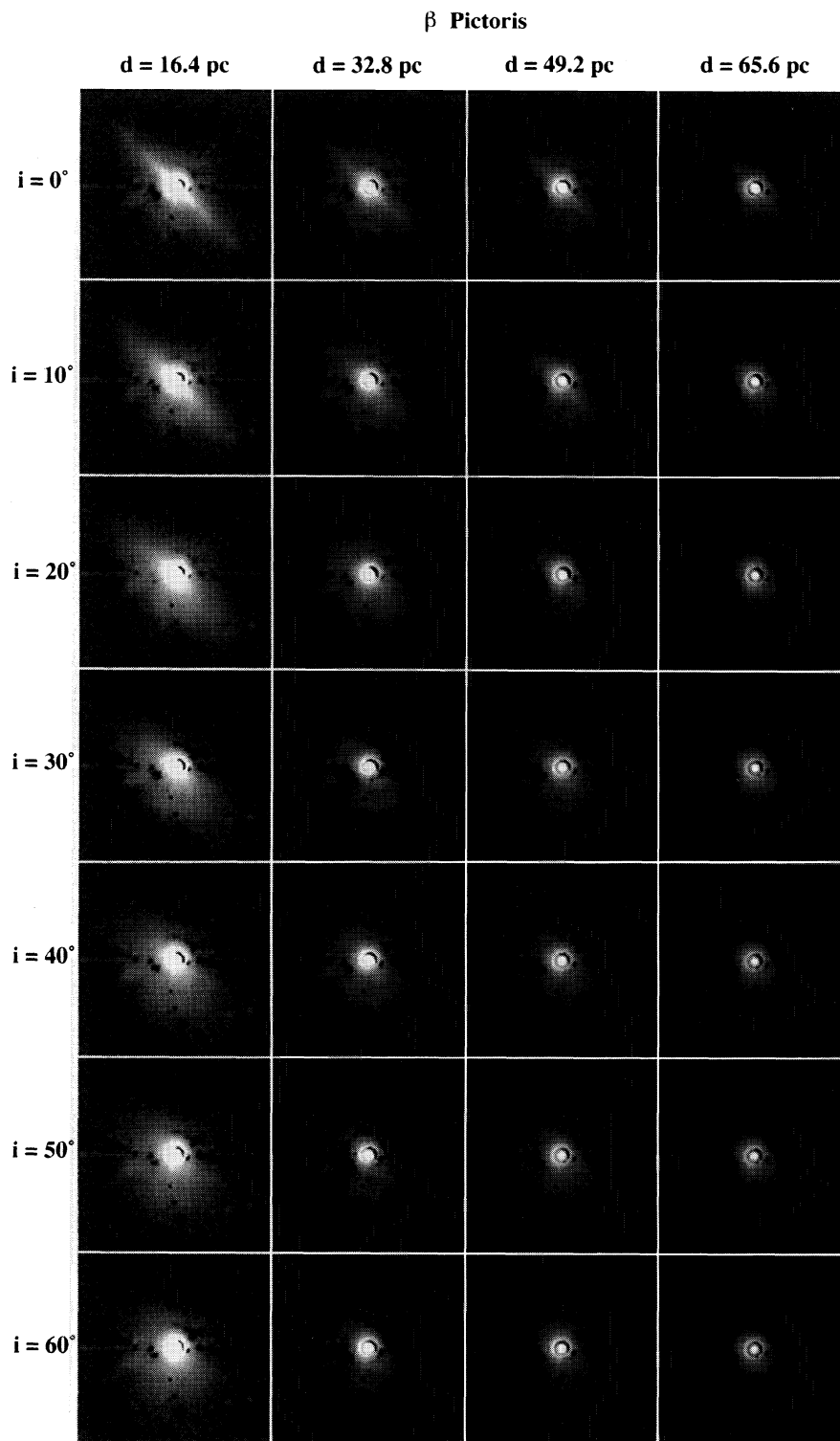
i = 40°

i = 50°

i = 60°

FIG. 5. The effects of inclination and distance on disk detectability. Model disks with a Henyey–Greenstein phase function ($|g|=0.5$) are inserted at P.A.=45° into R-band coronagraphic images of the β Pic surrogate star HR 1338, and then reduced by the same methods employed for β Pic. We show the logarithm of the final images with disk inclination increasing down columns and stellar distance increasing across rows. We do not present the $70° \leqslant i \leqslant 90°$ simulations because they are similar to the $i=60°$ simulation. Individual frames have a $80'' \times 80''$ field of view, north is up and east is left, and the background is limited by scattered light from the star.
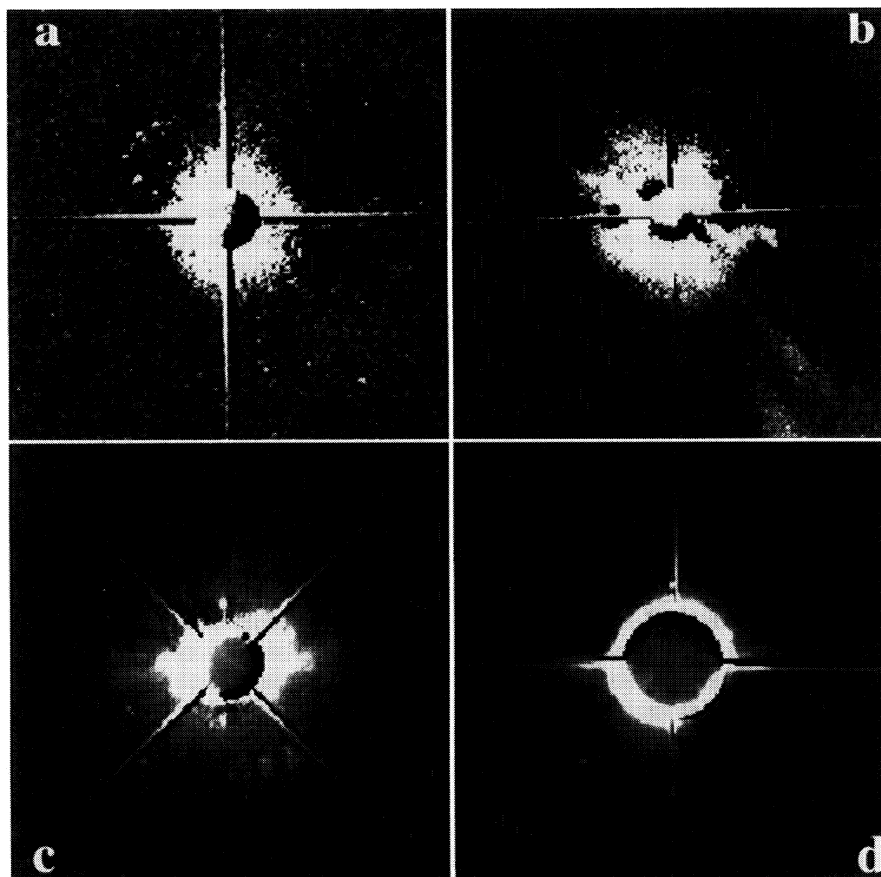
P. Kalas and D. Jewitt (see page 1350)

PLATE 45

FIG. 6. Logarithmic images of our reduced R-band Vega and Fomalhaut data (north is up, east is left). Panel (a) shows Vega (panel dimensions are $40''\times40''$) with the occulting spot blocking only $\sim2.5''$ (~20 AU) radius around the star. The residual halo of light within $\sim2''$ of the edge of the occulting spot could not be subtracted with the comparison star without oversubtracting the region beyond the halo. The halo may be due to a steeper PSF around Vega than the comparison star, or extra light scattered by circumstellar dust. Panels (b), (c), and (d) show reduced images of Fomalhaut using $4.0''$, $12.0''$, and $17.5''$ occulting spots, respectively. Panel (b) has dimensions $40''\times40''$ while panels (c) and (d) have dimensions $80''\times80''$. We find no nebulosity attributable to circumstellar dust in these images of Fomalhaut. The excess light to the southwest of the star in panel (b) is due to imperfectly cancelled instrumental scattering. Excess light in the east-west direction in panels (c) and (d) is also due to instrumental scattering as evidenced by its presence in comparison star images taken on the same nights.

P. Kalas and D. Jewitt (see page 1351)